Biochimica et Biophysica Acta 1838 (2014) 739–746

Contents lists available at ScienceDirect

Biochimica et Biophysica Acta

journal homepage: www.elsevier.com/locate/bbamem

The structure of the CD3ζζ transmembrane dimer in lipid bilayers

Satyan Sharma [a], Marc F. Lensink [b], André H. Juffer [a,*]

[a] Department of Biochemistry & Biocenter Oulu, University of Oulu, Oulu 90014, Finland
[b] Interdisciplinary Research Institute, CNRS USR3078, 50 avenue de Halley, F-59658 Villeneuve d'Ascq, France

ARTICLE INFO

Article history:
Received 6 May 2013
Received in revised form 26 November 2013
Accepted 2 December 2013
Available online 9 December 2013

Keywords:
Molecular dynamics
CD3ζζ transmembrane domain
T cell receptor
TCR–CD3 complex

ABSTRACT

Virtually every aspect of the human adaptive immune response is controlled by T cells. The T cell receptor (TCR) complex is responsible for the recognition of foreign peptide sequences, forming the initial step in the elimination of germ-infected cells. The recognition leads to an extracellular conformational change that is transmitted intracellularly through the Cluster of Differentiation 3 (CD3) subunits of the TCR–CD3 complex. Here we address the interplay between the disulfide-linked CD3ζζ dimer, an essential signaling component of the TCR–CD3 complex, and its lipidic environment. The disulfide bond formation requires the absolute presence of a nearby conserved aspartic acid, a fact that has mystified the scientific community. We use atomistic simulation methods to demonstrate that the conserved aspartic acid pair of the CD3ζζ dimer leads to a deformation of the membrane. This deformation changes the local environment of the cysteines and promotes disulfide bond formation. We also investigate the role of a conserved Tyr, highlighting its possible role in the interaction with other transmembrane components of the TCR–CD3 complex.

1. Introduction

The T cell receptor (TCR), in association with several CD3 (Cluster of Differentiation 3) subunits, forms a multimeric integral membrane complex, known as the TCR–CD3 complex, which is essential for the development and proper functioning of T cells [1]. The TCR is a heterodimer consisting of a TCRα and TCRβ chain, linked to each other through a disulfide bridge. Each chain contains an extracellular immunoglobulin (Ig) domain, a helical transmembrane (TM) domain, and a very short cytosolic region. The Ig domain of both chains jointly forms the "ligand binding domain" that interacts with the antigenic peptide bound to the major histocompatibility complex (MHC) resulting in T cell activation, which further requires the association of TCR with CD3 subunits. The invariant CD3 chains are present as CD3δε and CD3γε heterodimers and a CD3ζζ homodimer [2,3]. Each CD3 subunit has an extracellular domain that interacts with the extracellular domain of TCR. Although the three-dimensional structures of the extracellular domains of the TCR and CD3 dimers have been solved individually, many questions remain open as to the structural features of the organization of the TCR–CD3 complex. The intracellular domains of the CD3 subunits are of varying length and are connected to the extracellular domain via a helical TM domain spanning the membrane only once. The intracellular region of the CD3 subunits harbors the immunoreceptor tyrosine-based activation motif (ITAM). Upon antigen binding by TCRαβ, the ITAMs are phosphorylated and initiate a signaling cascade leading to T cell activation, the determinants of which are still unclear [1].

To date a number of mechanisms for TCR–CD3 receptor-mediated signaling have been proposed [4–6]. The importance of the TM helices in the receptor complex assembly has been highlighted by the novel finding of the role of the conserved, intramembrane ionizable residues in the association of these TM helices [7,8]. This feature has been shown to be valid for the assembly of other immunoreceptor complexes as well [9,10]. The TM domain of TCRαβ contains a set of three basic residues: an Arg and a Lys in TCRα and a Lys in TCRβ. The TM domain of each CD3 monomer contains a single acidic residue (Asp or Glu). Each basic residue on the TM domain of TCR is involved in an interaction with the pair of acidic residues present in one of the resulting CD3 dimers [11,12]. Mutations of any of the residues involved in this interaction result in a reduced association between TCR and CD3 [7]. These polar transmembrane contacts have also been suggested to be involved in the transmission of the ligand-induced conformational changes in the extracellular domains to the cytoplasmic domains, thus they are important for receptor-mediated signaling as well [11]. Further investigation of the structural features and dynamics of the transmembrane regions in their native environment would provide a deeper understanding of the association of the subunits and lead to a greater insight into the transmembrane interactions relevant to interdomain communications in the complex.

The CD3ζζ is the most striking component of the TCR–CD3 complex. The CD3ζ chain bears no similarity to any other CD3 monomer and it has a short extracellular domain comprising only nine amino acids. Absence of CD3ζ, or mutations in the transmembrane domain of CD3ζ, results in a failure of the surface expression of a functional TCR complex [13,14]. In spite of its short extracellular domain, the CD3ζζ dimer plays a dominant role in signaling as it contains 6 out of the 10 ITAMs found in the entire TCR–CD3 complex.

* Corresponding author. Tel.: +358 294 481161; fax: +358 8553 1141.
E-mail address: Andre.Juffer@oulu.fi (A.H. Juffer).

0005-2736/$ – see front matter © 2013 Elsevier B.V. All rights reserved.
http://dx.doi.org/10.1016/j.bbamem.2013.12.001

The structure of CD3ζζ, in a mixture of dodecyl phosphocholine sodium dodecyl sulfate (DPC SDS), has recently been solved using NMR (PDB ID: 2HAC) [15]. The NMR ensemble shows CD3ζζ to be a covalent dimer with an inter-chain disulfide bond involving conserved cysteines (labeled as position 2) near the membrane surface. Four residues C-terminal to these, a conserved aspartic acid is found at position 6. The conserved aspartic acid (Asp6/Asp6*) pair of the dimer has been suggested to be important for the formation of a covalently linked CD3ζζ. Earlier studies have shown that the disulfide-linked dimer can also be formed if both aspartic acid residues are replaced by any other charged residue, either positive or negative, or if aspartic acid is present at two, three or four residues C-terminal to the Cys [16]. This Asp6/Asp6* pair of the dimer is proposed to interact with the Arg of TCRα. It has also been shown that a charged and a polar residue pair at positions 6 are sufficient to form a covalently linked CD3ζζ [15]. The requirement of either a charged or a polar residue adjacent to Cys for disulfide bond formation is puzzling if not perplexing.

The NMR structure of CD3ζζ also shows that there are several polar and nonpolar contacts between the monomers in the membrane-spanning region. It is, however, undetermined whether the micellar structure is similar to the structure in lipid membranes, and whether or not the polar contacts are still preserved in the membrane environment.

We hypothesize that monomeric CD3ζ is inserted in the membrane with the aspartic acid bearing a net negative charge. Following insertion, the monomers associate to form a dimer. Subsequently, the dimers are covalently linked via a disulfide bridge. The formation of a disulfide bond effectively places the conserved aspartic acid residues of the monomers in close proximity to each other, as is observed in the recent NMR structure. This leads to important questions as to (*a*) what is the protonation state of each of these two Asps in the dimer, (*b*) what is their possible role in forming the disulfide-linkage and, (*c*) do the aspartic acids have any effect on the integrity of the bilayer and on the local environment of the cysteines? Although it has been suggested that the effects on membrane are important for the disulfide bridge formation [16,17], there is no direct experimental evidence for this.

In the present study, we have used extensive atomic-detail, molecular dynamics (MD) simulations to provide a detailed description of the molecular interactions involved and to address the aforementioned issues.

2. Materials and methods

2.1. MD simulations

A representative structure was chosen from the ensemble of NMR structures (PDB ID: 2HAC) [15], such that coiled regions at the termini of the protein were extended. The amino acid sequence is Ace-D^{-3} SKLCYLLDGILF^{10} IYGVILTALF^{20}LRVKFSRSAD^{30}-NH2, with the numbering scheme same as in the NMR structure. Note that the second chain of the dimer is referred to by an asterisk mark in the text.

The protein was inserted into a lipid bilayer consisting of 126 POPE molecules using the InflateGRO method [18]. Approximately 8500 water molecules were added to the system box ($7 \times 7 \times 10$ nm^3) such that no water molecules were placed in the interior of the bilayer. An appropriate number of ions was added to achieve electroneutrality. The system was then subjected to 1000 steps of steepest descent energy minimization and 100 ps of MD using weak position restraint (10^3 KJ/nm^2) on the non-hydrogen protein atoms, followed by a production run. The simulation for each system (with a different charge state of aspartic acid or a mutation) was carried out in triplicates, starting from a random initial velocity and followed until 60 ns.

All simulations were carried out with the GROMACS package (version 4.0.7) [19]. Atomistic simulations were done with the ffG53a6 force field [20] and Berger parameters [21] for lipid tails. A 2 fs time step was employed. The partial charges of the POPE headgroup were taken from a recent work by Lensink et al. [22]. All bonds were constrained using the LINCS algorithm [23]. Water molecules were treated explicitly using the SPC water model and constrained using the SETTLE algorithm [24,25]. Pressure was kept at 1 atm using the Parrinello–Rahman barostat [26] and the temperature was set at 310 K using a Nosé–Hoover thermostat [27,28] with a coupling constant of 0.1 ps. Pressure coupling was applied semi-isotropically along the directions parallel and normal to the bilayer surface. Electrostatic interactions were calculated at every step with the particle-mesh Ewald method [29].

2.2. Analysis of hydrogen bond and salt bridges

The cumulative existence of a hydrogen bond was calculated for each trajectory and averaged over three trajectories. A hydrogen bond was considered to exist if the distance between the hydrogen atom and acceptor was less than 2.5 Å with a donor–hydrogen–acceptor angle smaller than 60°.

The lipid–protein interactions were determined using a simple distance criterion. A salt bridge was considered when the distance between the lipid amine-nitrogen and residue oxygen atoms was less than 3 Å. Similarly, a 4 Å distance cut-off was used between the lipid phosphorus and residue-nitrogen atoms for a phosphate-residue salt bridge. Last 10 ns of three trajectories were combined and the cumulative presence (Δt_{cumul}) of salt bridges was calculated as combined fractional presence over the concatenated trajectory. The persistence factor *F* was calculated as described previously, using values of 0.51 and 3.16 nm^2 for MSF_{min} and MSF_{max}, respectively, see Ref. [22]. The residue conservation is calculated as before [22], using an *E*-value threshold of $1.0e^{-3}$.

3. Results

3.1. Dynamics and stability of disulfide linked dimers

To quantify the stability and the dynamics of the CD3ζζ dimer in a membrane environment, a series of molecular dynamics simulations of the dimer was carried out in a neutral and pre-equilibrated bilayer consisting of 1-palmitoyl-2-oleoyl-sn-glycero-3-phosphoethanolamine (POPE) lipids. The simulations were performed for three different charge states of the Asp6/Asp6* pair: −2 (both aspartic acids charged), −1 (Asp6 charged and Asp6* neutral) and neutral (both aspartic acids neutral). The resulting trajectories were analyzed for the changes in the secondary structure, the helix–helix crossing angle, the root-mean-square fluctuations, and distances between relevant residues and their atoms.

A secondary structure analysis with DSSP [30] shows all helices to retain their helical structure as observed in NMR experiments (data not shown). The secondary structure profile was found to be same for all three charge states.

To characterize the dimer association, the crossing angle between the two helices of the dimer was calculated. The crossing angle is a measure for the relative orientation of the helices with respect to each other. The mean crossing angle over the entire simulation length of the three states is 22° ± 2° for the −2 charge state, 23° ± 2° for the −1 charge state, and 25° ± 2° for the neutral state. A crossing angle of 23° has been reported for the NMR structure. Simulation studies of GpA dimers in lipid bilayers have shown that the dimers tend to have a larger value of the crossing angle in a micellar environment in comparison to the bilayer environment [31]. Although the structure of CD3ζζ was solved in a micellar environment, the simulations in this work show a similar value of crossing angle in the bilayer with a slight dependency on the actual charge state. The negligible change in crossing angles in the micelle and in the bilayer could be due to the fact that the monomers are crosslinked via a disulfide bond. In addition, the surface area of monomer–monomer contacts is much larger in CD3ζζ as compared to GpA. The DSSP and crossing angle analysis indicate that the overall backbone structure and dynamics are very similar in all the three charge states.

A set of averaged interatomic distances was calculated to describe the local geometric features of the Asp6/Asp6* pair for the three charge states (Table 1). The analysis shows that in the −2 charge state the distance between the aspartic acid carboxyl oxygens has increased significantly (from 2.5 to 6.5 Å). The distance between the Cys2 backbone O and the backbone H atom of Asp6, which is the i + 4th residue, is also larger in the −2 charge state. This indicates a distortion in the α-helical geometry in this region. In contrast, in the other two charge states the two aspartic acids remain close together via a persistent hydrogen bond between the protonated Oδ atom of one of the Asps and the unprotonated Oδ atom of the other. Although in the −1 charge state the distance between Asp6 Oδ and Asp6* N is larger with respect to the 0 (neutral) state, which is due to the insertion of a lipid headgroup in between the two aspartic acids (Fig. 1B), the two carboxyl groups still remain in close proximity. Moreover, the backbone hydrogen bonds between the main chain N–H of both aspartic acids and the main chain carbonyl group of Cys are consistent with a helical structure as observed by NMR. This leads us to conclude that the two aspartic acids are stabilized via a hydrogen bond between them. To ascertain the most probable charge state of the aspartic acid residues in the NMR structure, these computed distances were compared to the distances listed in Ref. [15] and in Table 1. From the data in Table 1 it can be noted that the distances for the 0 charge state are also close to the observed distances in the NMR structure, but we conclude that the −1 charge state is most likely, because of the experimental observation that a double mutation of the aspartic acids to Asn or Ser impairs dimer formation [15], making it unlikely that both aspartic acids be protonated in the 0 charge state. Altogether the results lead to the proposition that the charge state is indeed −1, i.e., one of the aspartic acids is protonated and the other is not.

In the NMR structure, inter-chain hydrogen bonds are observed between residues Tyr12–Thr17* and Tyr12*–Thr17 [15]. Mutations of these conserved residues lead to a drastic reduction in dimerization of the monomers. The MD simulation trajectories were analyzed for distance evolution between the Tyr Oη of one chain and Thr Oγ of the other for all three charge states. The results are shown in Fig. 1A. It can be seen that the distance between Tyr12* Oη and Thr17 Oγ varies depending on the charge state of the Asp6/Asp6* pair. The hydrogen bond existence for −2, −1 and 0 charge states was 89%, 87% and 91%, resp., for Tyr12 Oη and Thr17* Oγ, whereas the values were 51%, 34% and 92%, resp., for Tyr12* Oη and Thr17 Oγ.

A visual inspection of the trajectory for the −1 charge state shows that the diminished existence of the hydrogen bond between Tyr12* Oη and Thr17 Oγ is due to the tail of a POPE lipid being sandwiched between the side-chains of the two helices, with its headgroup tightly anchored in between the Asp6/Asp6* pair (Fig. 1B). This is not observed for the other two charge states. It is evident that there is a correlation between the side-chain fluctuations and the charge states of the Asp, dictating how closely the lipids interact with the center of the helix.

As mentioned before, in the NMR structure both Tyr–Thr hydrogen bonds are observed. This is likely due to the fact that the structure was obtained in a micellar environment. Micelles display a relatively loose structure and the detergent molecules generally have a shorter hydrophobic tail. Thus, with the hydrophilic moiety of a detergent molecule interacting with the aspartic acid pair, its tail can no longer reach the Tyr12* and Thr17 residues. Consequently, the side-chains of both Tyr–Thr pairs would remain hydrogen bonded.

Table 1
The comparison of the interatomic distances for the three charge states during the last 10 ns of the simulations.

Distance (atom1:atom2)	NMR	−2	−1	0
Asp6 Oδ:Cys2 O	3.8 ± 0.3	3.64 ± 0.04	3.34 ± 0.03	3.09 ± 0.03
Asp6 Oδ:Asp6* Oδ2	2.5 ± 0.1	6.51 ± 0.20	2.65 ± 0.01	2.66 ± 0.02
Asp6 Oδ:Asp6* N	4.0 ± 0.1	6.13 ± 0.16	5.49 ± 0.04	3.93 ± 0.06
Asp6* H:Cys2* O	2.1 ± 0.1	5.84 ± 0.15	2.13 ± 0.03	2.07 ± 0.04
Asp6 H:Cys2 O	–	3.84 ± 0.17	2.35 ± 0.04	2.01 ± 0.02

NMR distances are as listed in Ref. [15]. The values are in Å and shown as mean ± standard deviation. (–) not listed in Ref. [15].

3.2. Membrane and solvent dynamics

Upon further investigation of the lipid bilayer environment in the immediate vicinity of the TM peptides, we have noticed a strong interaction with local lipid phosphate groups and their relative displacement toward the interior of the bilayer. This is illustrated in Fig. 2, where a visualization of snapshots from the simulations shows that individual lipid headgroups are pulled toward the aspartic acid residues with the degree of penetration of the lipid headgroups toward the hydrophobic core clearly depends on the charge state of Asp6/Asp6*.

Fig. 3 shows the frequency of hydrogen bond formation between the side chain of the Asp6/Asp6* pair and the POPE headgroups. The aspartic acid pair forms two hydrogen bonds to lipid headgroups in the −2 and −1 charge states, and none in the 0 charge state. The same analysis for hydrogen bonds to water is also shown in Fig. 3. Virtually no hydrogen bonds to water are present in the −1 charge state, only a single water molecule is in the vicinity of the aspartic acid pair in the 0 charge state, whereas a multitude of water molecules can be found around the aspartic acid pair in the −2 charge state. We conclude that the presence of a charge is required on the aspartic acid pair to attract a lipid headgroup. For the −2 charge state, the two negatively charged aspartic acids distort the membrane to a greater extent, allowing a larger permeation of water inside the bilayer. We would like to stress that the permeation is localized to only the few lipid molecules, thus avoiding large-scale effects like bilayer thinning or even leaking.

Fig. 4 shows the details of interaction of lipid headgroups and the waters with the aspartic acid pair in the −2 and −1 charge states. In the −2 charge state, the repulsion between the two aspartic acids is stabilized by waters entering the lipid bilayer and dimer structure (see also Fig. 3B); the sidechains of both aspartic acids are bridged by a water (W1 in Fig. 4A). In addition, the Oδ atoms of each aspartic acid simultaneously interact with the headgroups of lipids (Asp6–POPE125 and Asp6*–POPE166) and an additional water (Asp6–W2 and Asp6*–W3). In the −1 charge state, the two aspartic acids remain closer to each other (Table 1) with one of the oxygens of Asp6 being hydrogen-bonded to the Oδ carboxyl hydrogen of neutral Asp6*. In addition, instead of interacting with different lipid headgroups, the two aspartic acids now simultaneously interact with the same lipid headgroup (Figs. 1B and 2B).

The fact that in the probable physiological, −1 charge state, both aspartic acids simultaneously interact with the same lipid headgroup has led us to conduct a thorough investigation of lipid–protein interactions. We have decided to follow our previous definition of persistent lipid–protein interaction to investigate only the strongest interactions. In short, the method classifies lipid-mediated salt bridges combining hydrogen bonding with spatial fluctuation of interacting groups. The persistence factor *F* is a measure of the strength of the interaction and a high persistence factor may be indicative of specific binding.

Table 2 shows 7 lipid-mediated salt bridges with a cumulative presence of 5%. Last 10 ns of each of the three independent trajectories were combined and the analysis was carried out on this combined trajectory. Most observed interactions include residues located at the extremes of the helix, e.g. Asp-3 on the acceptor side and Arg22 on the donor side. The corresponding persistence factors of 31.6/33.0 for Asp-3/Lys-1 and 16.0/15.8 for Tyr3/Lys-1 indicate a high level of significance. Their non-divergence means similar strength of interaction at donor and acceptor side of the lipid-mediated salt bridge. It is not surprising to see these residues undergo interactions with lipid headgroups as it is these residues that are responsible for the anchoring of the peptide in the bilayer. We would like to stress that a lipid-mediated salt bridge is not required for such anchoring, see e.g. the case of Asp30/Arg22 where we do not consider the interaction with Asp30 relevant

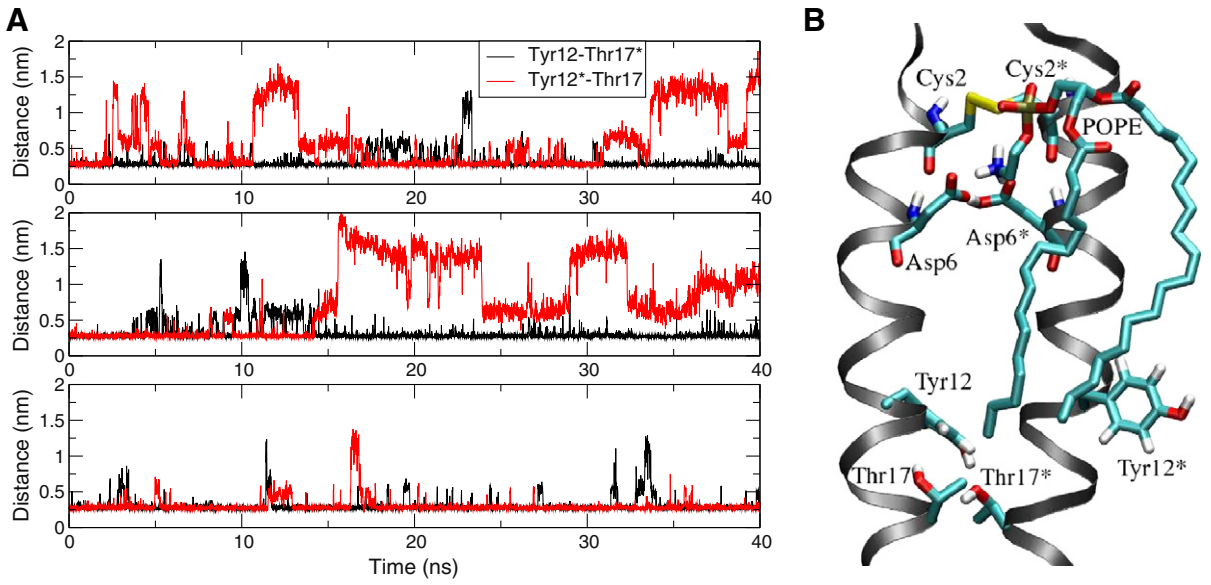

Fig. 1. The interaction between Tyr Oη and Thr Oγ. (A) Distance between the Tyr Oη and Thr Oγ atoms in −2 (top), −1 (middle) and 0 (bottom) charge states. (B) Snapshot of the insertion of POPE in between Ty12* and Thr17 for the −1 charge state. The dashed lines depict the hydrogen bonds.

(see below). Also the interaction with Lys-1 is likely to carry relevance as the residue is moderately conserved at that position (60% Lys, 12% Arg, 17% Gln), but we do not consider the interactions with Ser-2 and Asp30 family-specific. Although the interaction of the C-terminal Asp30 involves both side chain and C-terminal charge, the residue is located away from the helix end point and it is not conserved (54%). Likewise, Ser-2 is a proline in close to 83% of the sequences.

Besides the anchoring interaction of Asp-3, Arg22 and Tyr3, one additional bridge stands out, namely the double bridge over POPE125 from Asp6/Asp6* to Tyr3. Both Asp6 and Asp6* act as hydrogen bond acceptor to the POPE amine group. The phosphate group of the same lipid is acceptor to the hydroxyl hydrogen of Tyr3. In addition, the hydroxyl oxygen of the same Tyr3 residue is acting as hydrogen bond acceptor to the POPE140 amine group. It should be noted that also Tyr3* is involved in a lipid-mediated salt bridge, acting as hydrogen bond donor in the bridge to Asp-3*. All residues in the interacting motif around POPE125, Asp6, Asp6* and also Tyr3, are highly conserved. Interestingly, the mutation of Tyr3 to Ala is known to lead to a significant reduction in dimer formation [15]. We believe that the interacting motif is indicative of the mode of interaction of the CD3ζζ dimer with the transmembrane arginine on the TCRα, which is important for the assembly of a functional TCR–CD3 complex.

3.3. Non-crosslinked dimer and mutants

As mentioned before, the conserved Asp6/Asp6* pair is only required for the disulfide linkage and not for the initial association of the monomers [15]. For example, a significant reduction in the amount of covalently linked CD3ζζ for the Ala6/Ala6* mutant has led to the suggestion of local membrane deformation being involved in the disulfide bond formation [16,17]. To conclusively show that 1) the free monomers remain closely associated even in the presence of negatively charged Asp, and 2) there is indeed an appreciable membrane deformation only in the presence of a charged residue, atomistic simulations

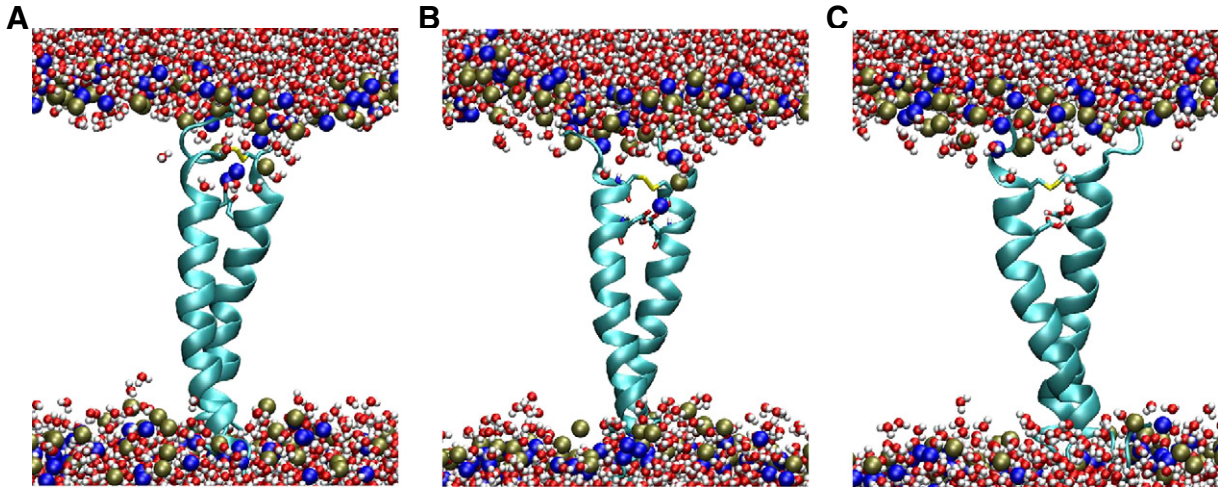

Fig. 2. The penetration of PE phosphate groups toward the interior of the lipid bilayer and associated water defects. The snapshots are shown from the simulations of (A) −2 charge state, (B) −1 charge state, and (C) 0 charge state. The lipid phosphate and nitrogen atoms are shown as brown and blue spheres. The water oxygen and hydrogen atoms are shown as red and white spheres. Also shown are the disulfide linked Cys2/Cys2* and the Asp6/Asp6* pair in stick representation. Note the 2 (A, −2) and single (B, −1) lipid molecules interacting with the aspartic acid negative charge.

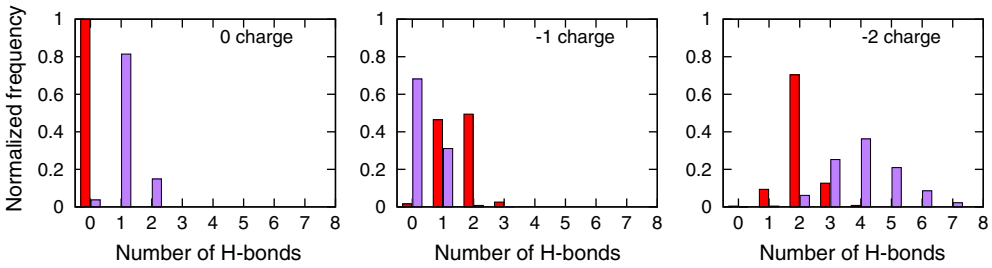

Fig. 3. Normalized frequency of hydrogen bonds formed by the Asp6/Asp6* pair with either lipid headgroup (red) or water molecules (purple) over the entire simulations (in triplicates) for 0 (left), −1 (middle), and −2 (right) charge states.

were carried out with Asp6/Asp6* and Ala6/Ala6* dimers. In these simulations two monomers were closely placed in a POPE bilayer with both cysteines reduced. Furthermore, to understand the effect of other mutations, which have been previously studied experimentally [15], four additional simulations of non-covalently linked dimers were carried out in triplicates. In these simulations, either one of the aspartic acid was mutated to Ser (Asp6/Ser6*), or to Ala (Asp6/Ala6*) or both the aspartic acids were mutated to Ala (Ala6/Ala6*). The non-covalently linked wild type dimer (Asp6/Asp6*) was also studied. The aspartic acids were charged, representing a −2 charge state. Each simulation was carried out for 60 ns.

The interhelical distance was employed as a measure to assess the stability of the association of the monomers in the dimer. Fig. 5 shows the interhelical distance between the monomers for the Asp6/Asp6* and Ala6/Ala6* simulations. As can be seen the two monomers remain associated over the entire length of the simulation, in spite of the absence of the disulfide linkage. The results are in agreement with the experimental observation that the inter-chain disulfide bond is not the main contributor to the dimerization. Fig. 6 shows that there is indeed a larger degree of membrane destabilization due to phosphate moieties penetrating the lipid bilayer for Asp6/Asp6* with respect to Ala6/Ala6*. It is interesting to note that both of the Tyr–Thr hydrogen bonds remain intact in the Ala6/Ala6* mutant, whereas only one of them persists in Asp6/Asp6*.

For the various mutants and wild type simulations, the average distance *d* between the phosphate atoms of the upper leaflet of the bilayer and the center of the hydrophobic core (see also Fig. 6) is plotted as a function of radial distance *r* from the center of the CD3ζζ dimer (Fig. 7). The center of the bilayer was calculated as the mean position of the tail particles of both monolayers of the bilayer. It can be seen that largest deformation occurs for Asp6/Asp6* (corresponding to a −2 charge state). The presence of negative charge pulls the positively charged headgroups of nearby POPE lipids into the bilayer, leading to deformation and decrease in thickness of the upper layer of the bilayer around the transmembrane helices. This dipping in the membrane would in fact expose the Cys involved in disulfide bond formation. The smallest deformation is observed for Ala6/Ala6*. The presence of aspartic acid in one of the monomers is sufficient to disrupt the bilayer and increase the exposure of Cys to solvent, which is an absolute requirement for its oxidation. The deformation of the bilayer for the Asp6/Ser6* mutant appears comparable to Asp6/Asp6*. A mutation at this position to Ala abolishes the lipid–protein interaction. These simulations strongly substantiate the requirement of a charged group in the vicinity of the cysteines. The substitution of aspartic acid at position 5 or 7 would still allow bilayer deformation. However, mutants with a charged group at a position beyond 6 or 7 would probably introduce a kink in the helix and disfavor dimer formation. The presence of a positively charged residue such as Arg would likely also result in a deformation of the bilayer as the positive charge on Arg could interact favorably with the lipid phosphate group. However, due to the location of the phosphate moiety being intrinsically closer to the bilayer center with respect to the PE amine group, together with the longer and less restrained Lys or Arg side-chain, the bilayer deformation would be significantly smaller.

The "curving-in" of the membrane near the CD3ζζ dimer also leads to an increase in the number of positively charged headgroup moieties in the vicinity of Cys, as depicted in Fig. 8, where we show the number of POPE amine groups in contact with both cysteines. The figure shows that there are significantly more contacts in the case of Asp6/Asp6* or Asp6/Ser6* with respect to the Ala6/Ala6* mutation.

4. Discussion

Using a series of MD simulations, we have performed a systematic study of the structure and dimerization of CD3ζζ in a POPE lipid bilayer. It is important to consider that the results of a simulation study depend on the fore field employed. In the present study, we used a combination of ffG53a6 force field [20] and Berger lipid parameters [21]. The ffG53a6

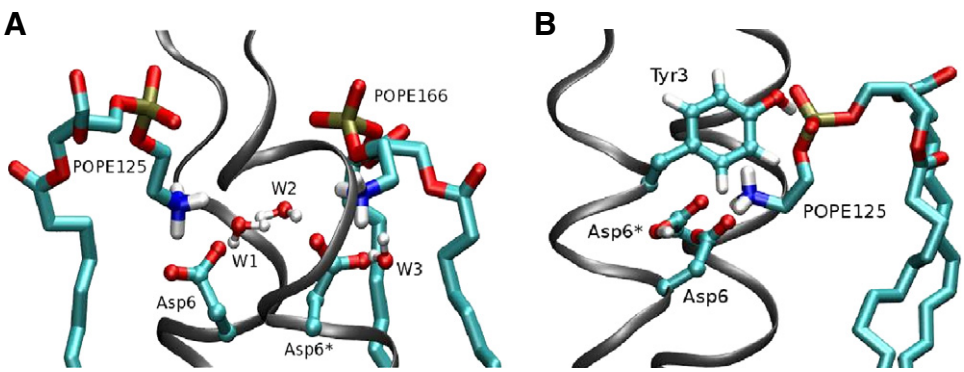

Fig. 4. The interactions of POPE headgroups and waters (if any) with the two aspartic acids. The details are shown for (A) −2 charge state, and (B) −1 charge state. The interaction between Tyr3 and POPE125 is also highlighted.

Table 2
Lipid mediated salt bridges with a cumulative presence (Δt) of more than 5%.

Acceptor		Lipid	Δt_{cumul}	$F_{acceptor}$	F_{donor}	Donor	
	(a)		%				(a)
Asp-3	92.4	POPE106	44.7	31.6	33.0	Lys-1	71.7
Asp30	54.4	POPE154	33.2	7.8	7.7	Arg22	93.5
Asp6	93.5	POPE125	23.5	12.0	11.6	Tyr3	93.5
Tyr3	93.5	POPE140	21.4	16.0	15.8	Lys-1	71.7
Asp-3	92.4	POPE145	16.0	6.9	6.6	Ser-2	6.5
Asp6*	93.5	POPE125	8.6	4.4	4.2	Tyr3	93.5
Asp30	54.4	POPE140	5.3	3.1	3.4	Asp30[b]	54.4

[a]Residue conservation in %.
[b]C-terminal residue.
*Note that residue numbering can be negative as in PDB ID: 2HAC [15] and an asterisk mark refers to the second chain of the dimer.

force field was recently included in an evaluation of microsecond molecular dynamics simulation and showed a stability that was on par with Amber [32]. Unfortunately force field reviewing literature currently lacks a systematic study of peptide stability in the presence of a lipid environment, but the ffG53a6 force field is routinely used in combination with Berger lipid parameters, yielding reproducible results that are in agreement with experimental observations [33–35].

Since recent studies have shown that in the covalently linked CD3ζζ dimer the conserved Asp6 from each monomer lies in close proximity of each other [15], important questions were raised as to the protonation state of these Asps, their possible role in forming a disulfide-linkage, and their effect on the integrity of the bilayer and on the local environment of the cysteines. It has been argued that each aspartic acid residue of the pair would be charged and stabilized via hydrogen bonds to a water molecule. The existence of a stabilizing water was suggested on the basis of a weak signal in NMR studies [15], but further details and studies are lacking.

In the present work three representative charge states were considered: −2 (both aspartic acids charged), −1 (Asp6 charged and Asp6* neutral) and 0 (both aspartic acids neutral). The geometric comparison of the simulation results with the NMR structure strongly suggests that the Asp6/Asp6* pair exists in a −1 charge state. In essence this means that the two aspartic acids stabilize each other through an inter-Asp hydrogen bond. Such an arrangement is not unusual. In fact, a similar arrangement of the aspartic acid dyad has been reported for HIV-1 protease and Plasmepsin II [36,37]. In these two enzymes, it has been shown that the two closely positioned aspartic acids share a proton, similar to our findings. In addition, there is a water molecule simultaneously hydrogen-bonded to both. In our simulations, instead of a water molecule, we find the two aspartic acids to be involved in a strong electrostatic interaction with a single lipid headgroup, also involving the conserved Tyr3. The orientation of the aspartic acid side-chains is consistent with the NMR structure [15]. It is very likely that in the micellar structure, a water molecule could be positioned at this site, playing a similar role as the lipid headgroup. The present study provides an interesting view of the mode of interaction of the charged Asp6/Asp6* pair with the lipid headgroups in a neutral lipid bilayer. The comparison of the relative orientation of the two aspartic acids in various charge states, and their interaction with the lipid headgroup convincingly demonstrates that both aspartic acids can interact with a single positive charge if, and only if, they are stabilized through a shared proton.

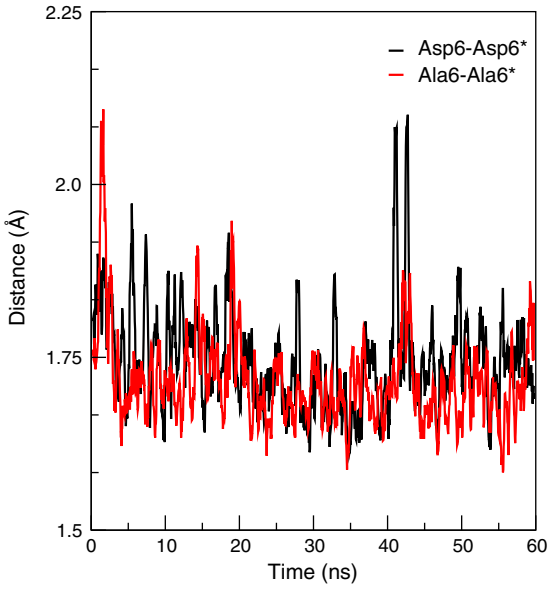

Fig. 5. The interhelical distance in the Asp6/Asp6* (black) and Ala6/Ala6* (red) mutants.

The simulations additionally demonstrate that of the two inter helix Tyr–Thr hydrogen bonds observed in the NMR structure, only one is persistent. The other Tyr–Thr pair interacts strongly with the lipid tail, and their interaction is more often disturbed. This in fact provides a sense of directionality in the mode of interaction of the CD3ζζ dimer with the TCR. Previous studies have shown that a mutation of the conserved Tyr results in signaling defects [38]. Simultaneously, the transmembrane aromatic residues can interact via π–π interactions within the membrane and, consequently, provide specificity [39]. Thus in a TCR–CD3 complex, one of the faces of the CD3ζζ dimer would interact through charge–charge interactions and, along the same face, the Tyr of the Tyr–Thr pair would interact with aromatic residues present on nearby helices in the TCR–CD3 complex. These results together increase our understanding of the functioning of the dimer in the assembled TCR–CD3 complex.

To form a disulfide bond, one of the prerequisites is that the cysteines that are participating in the disulfide bond are not buried in the membrane. They should be exposed to the lumen of the endoplasmic reticulum, accessible to the cellular machinery catalyzing the disulfide bond formation. At first, the requirement of a charged aspartic acid near the Cys for the formation of disulfide bond appears counterintuitive, even more so when the two residues lie on the same face of the helix. However, the extensive simulation of non-covalently linked dimers shows that these dimers are still stable, in spite of the nearby presence of similarly charged residues in both helices. Also, the dimer association appears nearly identical to the Ala6/Ala6* mutant. This finding is in agreement with the experimental observation that conserved aspartic acids are not involved in the initial association of the dimers [15], but rather, as demonstrated here, important for the formation of the disulfide bridge. In addition, our simulations show at the molecular level how this dependence could be explained.

Our results convincingly demonstrate that the presence of a charged aspartate residue near the membrane surface leads to a deformation of the lipid bilayer, thereby increasing the accessibility of the cysteines to the machinery catalyzing disulfide bond formation (Fig. 7). The presence of a serine in one of the positions of the aspartic acid (Asp6/Ser6*) is able to deform the bilayer to a similar extent. The membrane deformation results in an increase in the number of contacts of Cys with positively charged headgroups of the membrane and, consequently, increase the susceptibility of the Cys to donate protons, which in turn increase the likelihood of the two Cys to form a disulfide bond. The presence of uncharged residues at this position would suppress the bilayer deformation and result in a significantly lower solvent exposure of the cysteines, in accordance with the previous experimental observations [16,15]. We therefore conclude that the disulfide bond formation requires two conditions to be fulfilled, namely bilayer deformation and positioning of the both the cysteines near each other. The observation from the atomistic MD simulations that the degree of deformation of the bilayer depends on the charge state of the aspartic acid is confirmed by our coarse-grained (CG) simulations resulting in a larger solvent exposure of the Cys (data not shown).

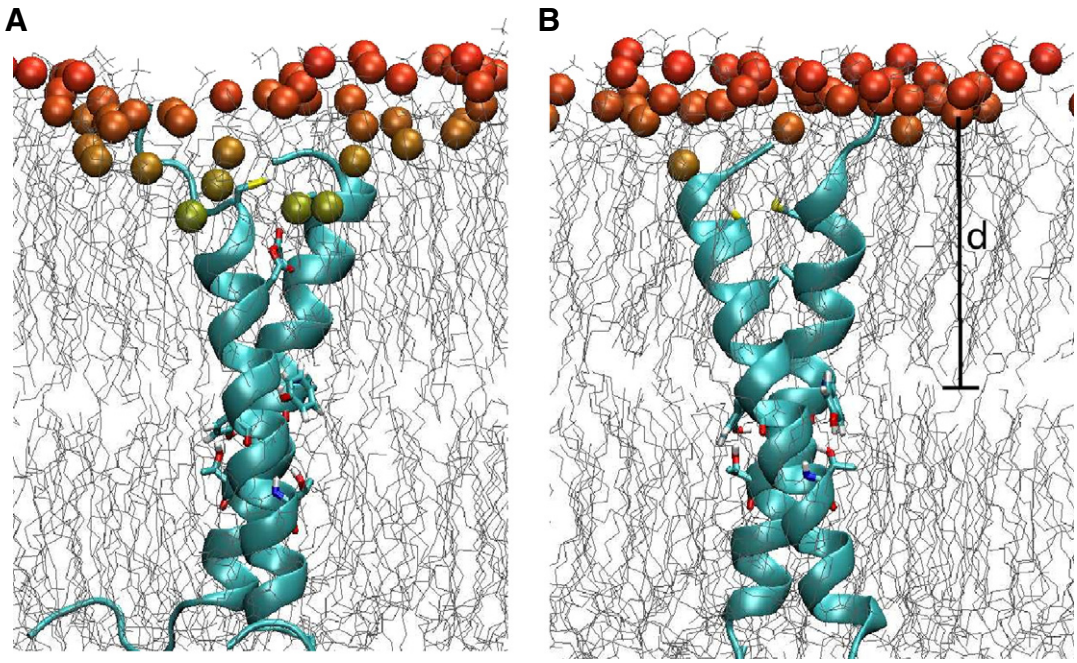

Fig. 6. Penetration of phosphate into the bilayer in (A) Asp6/Asp6* and (B) mutant Ala6/Ala6*. Also shown are the Tyr–Thr pairs lying close to the center of the bilayer.

Summarizing our observation with data from literature, the process of formation of the covalently linked CD3ζζ dimer could be envisaged as follows: the CD3ζ chains are independently inserted into the membrane of the ER and then self-assemble into non-covalent dimers [11]. The initial dimerization is mediated through strong polar interactions between the two helices. Specific polar interactions occur between the Tyr12 and Thr17* residues. In addition, Van der Waals interactions involving Leu9, Gly13, and Phe20 further stabilize the dimers. The role of the Asp6 on each of the monomer is to ensure that the Cys2/Cys2* pair is exposed to the membrane exterior, enabling the formation of the covalently linked dimer. The presence of the newly formed covalent disulfide bond near Asp6 places the two aspartic acids close to each other. An inter-aspartic acid hydrogen bond then further stabilizes the dimer. The Cys–Cys bond and Asp–Asp pair together form a rigid configuration of the CD3ζζ dimer near the extracellular surface of the membrane. The ligand-induced conformational changes in the TCR–CD3 complex, through interaction of TCRα TM Arg with the aspartic acid pair of the CD3ζζ dimer, can then be efficiently transferred through the small extra-cellular domain of ζζ to the intra-cellular ITAM domains via its closely packed TM helices.

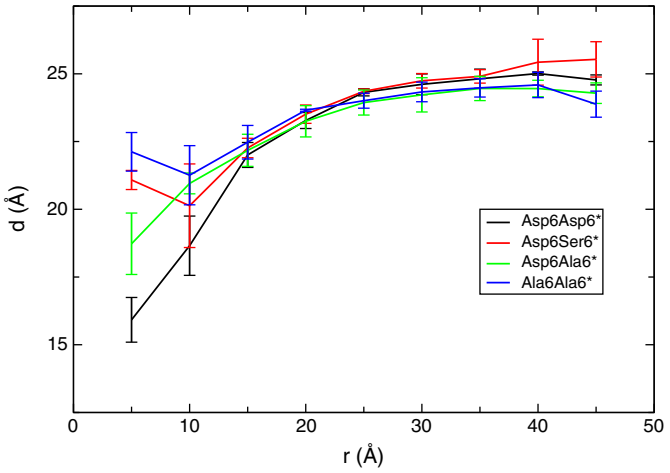

Fig. 7. Effect of various residues on the extent of bilayer deformation depicted as the distance *d* in Fig. 6 with respect to the radial distance *r*, from the center of mass of the dimer, for the Asp6/Asp6*, Asp6/Ser6*, Asp6/Ala6* and Ala6/Ala6* simulations.

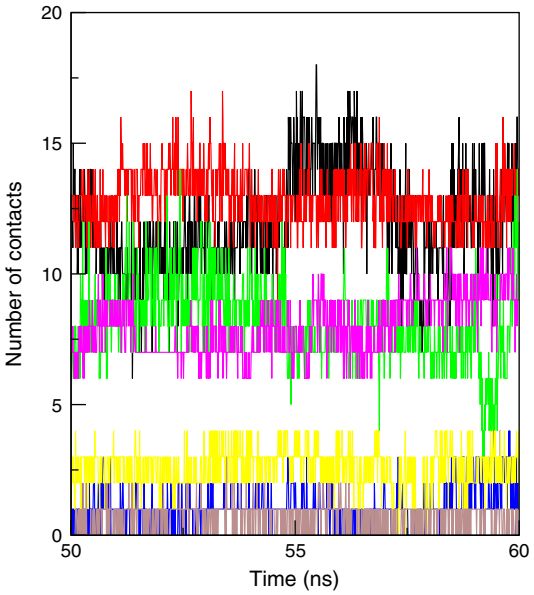

Fig. 8. Number of contacts of cysteines (Cys6 and Cys6*) with POPE amine nitrogen atoms, using a distance criterion of 6 Å over the last 10 ns of simulation time. The number of contacts is plotted for three simulations of Asp6Asp6* (black, red and green), Ala6Ala6* (brown, blue and yellow) and one simulation of Asp6Ser6* (magenta).

Acknowledgement

We thank the Center for Scientific Computing-IT Center for Science Ltd., Espoo-FI, for providing computational resources. We acknowledge the Biocenter Oulu Biocomputing Core Facility for financial support.

References

[1] J.E. Smith-Garvin, G.A. Koretzky, M.S. Jordan, T cell activation, Annu. Rev. Immunol. 27 (2009) 551–589.
[2] M.E. Call, K.W. Wucherpfennig, Molecular mechanisms for the assembly of the T cell receptor–CD3 complex, Mol. Immunol. 40 (2004) 1295–1305.
[3] M.G. Rudolph, R.L. Stanfield, I.A. Wilson, How TCRs bind MHCs, peptides, and coreceptors, Annu. Rev. Immunol. 24 (2006) 419–466.
[4] S. Minguet, W.W.A. Schamel, A permissive geometry model for TCR–CD3 activation, Trends Biochem. Sci. 33 (2008) 51–57.
[5] S.E. Levin, A. Weiss, Twisting tails exposed: the evidence for TCR conformational change, J. Exp. Med. 201 (2005) 489–492.
[6] M.S. Kuhns, M.M. Davis, K.C. Garcia, Deconstructing the form and function of the TCR/CD3 complex, Immunity 24 (2006) 133–139.
[7] M.E. Call, J. Pyrdol, M. Wiedmann, K.W. Wucherpfennig, The organizing principle in the formation of the T cell receptor–CD3 complex, Cell 111 (2002) 967–979.
[8] K.W. Wucherpfennig, E. Gagnon, M.J. Call, E.S. Huseby, M.E. Call, Structural biology of the T-cell receptor: insights into receptor assembly, ligand recognition, and initiation of signaling, Cold Spring Harb. Perspect. Biol. 2 (2009) a005140.
[9] J.A. Gosse, A. Wagenknecht-Wiesner, D. Holowka, B. Baird, Transmembrane sequences are determinants of immunoreceptor signaling, J. Immunol. 175 (2005) 2123–2131.
[10] J. Feng, D. Garrity, M.E. Call, H. Moffett, K.W. Wucherpfennig, Convergence on a distinctive assembly mechanism by unrelated families of activating immune receptors, Immunity 22 (2005) 427–438.
[11] M.E. Call, K.W. Wucherpfennig, Common themes in the assembly and architecture of activating immune receptors, Nat. Rev. Immunol. 11 (2007) 841–850.
[12] M.E. Call, K.W. Wucherpfennig, The T cell receptor: critical role of the membrane environment in receptor assembly and function, Annu. Rev. Immunol. 23 (2005) 101–125.
[13] C. Geisler, J. Kuhlmann, T. Plesner, B. Rubin, Failure to synthesize the human T-cell CD3-zeta chain and its consequence for the T-cell receptor–CD3 complex expression, Scand. J. Immunol. 30 (1989) 191–197.
[14] L. Bolliger, B. Johansson, Identification and functional characterization of the zeta-chain dimerization motif for TCR surface expression, J. Immunol. 163 (1999) 3867–3876.
[15] M.E. Call, J.R. Schnell, X. Chenqi, R.A. Lutz, J.J. Chou, K.W. Wucherpfennig, The structure of the ζζ transmembrane dimer reveals features essential for its assembly with the T cell receptor, Cell 127 (2006) 355–368.
[16] T. Rutledge, P. Cosson, J.S. Manolios, N. Bonifacino, R.D. Klausner, Transmembrane helical interactions: zeta chain dimerization and functional association with the t cell antigen receptor, EMBO J. 11 (1992) 3245–3254.
[17] S.J. Singer, The structure and insertion of integral proteins in membranes, Annu. Rev. Cell Biol. 6 (1990) 247–296.
[18] C. Kandt, W.L. Ash, D.P. Tieleman, Setting up and running molecular dynamics simulations of membrane proteins, Methods 41 (2007) 475–488.
[19] B. Hess, C. Kutzner, D. van der Spoel, E. Lindahl, GROMACS 4: algorithms for highly efficient, load-balanced, and scalable molecular simulation, J. Chem. Theory Comput. 4 (2008) 435–447.
[20] C. Oostenbrink, A. Villa, A.E. Mark, W.F. van Gunsteren, A biomolecular force field based on the free enthalpy of hydration and solvation: the GROMOS force-field parameter sets 53a5 and 53a6, J. Comput. Chem. 25 (2004) 1656–1657.
[21] O. Berger, O. Edholm, F. Jähnig, Molecular dynamics simulations of a fluid bilayer of dipalmitoylphosphatidylcholine at full hydration, constant pressure, and constant temperature, Biophys. J. 72 (1997) 2002–2013.
[22] M.F. Lensink, C. Govaerts, J.M. Ruysschaert, Identification of specific lipid-binding sites in integral membrane proteins, J. Biol. Chem. 285 (2010) 10519–10526.
[23] B. Hess, H. Bekker, H.J.C. Berendsen, J.G.E.M. Fraaije, LINCS: a linear constraint solver for molecular simulations, J. Comput. Chem. 18 (1997) 1463–1472.
[24] H.J.C. Berendsen, J.P.M. Postma, W.F. van Gunsteren, J. Hermans, Interaction models for water in relation to protein hydration, in: B. Pullman (Ed.), Intermolecular Forces, Reidel, Dordrecht, 1981, pp. 331–342.
[25] S. Miyamoto, P.A. Kollman, SETTLE: an analytical version of the SHAKE and RATTLE algorithms for rigid water models, J. Comput. Chem. 13 (1992) 952–962.
[26] M. Parrinello, A. Rahman, Polymorphic transitions in single crystals: a new molecular dynamics method, J. Appl. Phys. 52 (1981) 7182.
[27] S. Nosé, A unified formulation of the constant temperature molecular dynamics methods, J. Chem. Phys. 81 (1984) 44734–44742.
[28] W.G. Hoover, Canonical dynamics: equilibrium phase-space distributions, Phys. Rev. A 31 (1985) 1695–1697.
[29] U. Essmann, L. Perera, M.L. Berkowitz, T. Darden, H. Lee, L.G. Pedersen, A smooth particle mesh Ewald potential, J. Chem. Phys. 103 (1995) 8577–8592.
[30] W. Kabsch, C. Sander, Dictionary of protein secondary structure: pattern recognition of hydrogen-bonded and geometrical features, Biopolymers 22 (1983) 2577–2637.
[31] J.M. Cuthbertson, P.J. Bond, M.S. Sansom, Transmembrane helix–helix interactions: comparative simulations of the glycophorin a dimer, Biochemistry 45 (2006) 14298–14310.
[32] E.A. Cino, W.-Y. Choy, M. Karttunen, Comparison of secondary structure formation using 10 different force fields in microsecond molecular dynamics simulations, J. Chem. Theory Comput. 8 (2012) 2725–2740.
[33] M.J. Niesen, S. Bhattacharya, N. Vaidehi, The role of conformational ensembles in ligand recognition in G-protein coupled receptors, J. Am. Chem. Soc. 133 (2011) 13197–13204.
[34] C. Poojari, B. Strodel, Stability of transmembrane amyloid β-peptide and membrane integrity tested by molecular modeling of site-specific Aβ42 mutations, PLoS ONE 8 (2013) e78399.
[35] K. Berka, M. Paloncýová, P. Anzenbacher, M. Otyepka, Behavior of human cytochromes P450 on lipid membranes, J. Phys. Chem. B 117 (2013) 11556–11564.
[36] S. Piana, P. Carloni, Conformational flexibility of the catalytic asp dyad in HIV-1 protease: an ab initio study on the free enzyme, Proteins 39 (2000) 26–36.
[37] R. Friedman, A. Caflisch, The protonation state of the catalytic aspartates in plasmepsin II, FEBS Lett. 581 (2007) 4120–4124.
[38] S. Fuller-Espie, P.H. Towler, D.L. Wiest, I. Tiejen, L.M. Spain, Transmembrane polar residues of TCR beta chain are required for signal transduction, Int. Immunol. 10 (1998) 923–933.
[39] N. Sal-Man, D. Gerber, I. Bloch, Y. Shai, Specificity in transmembrane helix–helix interactions mediated by aromatic residues, J. Biol. Chem. 282 (2007) 19753–19761.